HHS Public Access

Author manuscript

Radiother Oncol. Author manuscript; available in PMC 2021 December 01.

Published in final edited form as:

Radiother Oncol. 2020 December ; 153: 106–113. doi:10.1016/j.radonc.2020.09.046.

ADC measurements on the Unity MR-linac – a recommendation on behalf of the Elekta Unity MR-linac consortium

Ernst S. Kooreman[a], **Petra J. van Houdt**[a], **Rick Keesman**[a], **Floris J. Pos**[a], **Vivian W.J. van Pelt**[a], **Marlies E. Nowee**[a], **Andreas Wetscherek**[b], **Rob H.N. Tijssen**[c], **Marielle E.P. Philippens**[c], **Daniela Thorwarth**[d], **Jihong Wang**[e], **Amita Shukla-Dave**[f], **William A. Hall**[g], **Eric S. Paulson**[g], **Uulke A. van der Heide**[a]

[a.]Department of Radiation Oncology, The Netherlands Cancer Institute, Amsterdam, The Netherlands [b.]Joint Department of Physics, The Institute of Cancer Research, and The Royal Marsden NHS Foundation Trust, London, United Kingdom [c.]Department of Radiotherapy, University Medical Center Utrecht, Utrecht, The Netherlands [d.]Section for Biomedical Physics, Department of Radiation Oncology, University of Tübingen, Tübingen, Germany [e.]Department of Radiation Physics, The University of Texas MD Anderson Cancer Center, Houston, United States [f.]Departments of Medical Physics and Radiology, Memorial Sloan Kettering Cancer Center, New York, New York, USA [g.]Department of Radiation Oncology, Medical College of Wisconsin, Milwaukee, United States

Introduction

Imaging biomarkers are important in oncology as they non-invasively provide information about the tumor and can be used for treatment response monitoring [1]. Quantitative imaging biomarkers (QIBs), are of particular interest because they provide quantitative information about tissue characteristics [2]. Ideally, they facilitate the comparison across different vendors and centers. However, differences in system hardware, acquisition parameters, and image analysis techniques introduce variability of QIB values [3,4]. It is critical to understand these differences and to test and validate QIBs before they can be incorporated in clinical trials [5].

The introduction of hybrid systems, which integrate an MRI with a linear accelerator (MR-linac), presents a unique opportunity for QIB studies. MRI-guided treatments enable QIBs to be acquired daily, which is practically not feasible on diagnostic MRI systems and will provide valuable longitudinal information. However, to maximize the power of these QIB studies, it is critical to harmonize the acquisition protocols across centers.

The apparent diffusion coefficient (ADC), derived from diffusion-weighted imaging (DWI), has been shown to change during treatment with radiotherapy [6–11]. Recently, efforts were made to standardize DWI acquisition. Initiatives like the quantitative imaging biomarkers alliance (QIBA), and other working groups have led to consensus recommendations for DWI

Corresponding author: Uulke van der Heide, Plesmanlaan 121, 1066 CX Amsterdam, The Netherlands, u.vd.heide@nki.nl.

in multiple tumor sites based on existing literature [12–14]. However, these recommendations are specifically designed for diagnostic MRI systems, while MR-linacs may warrant additional considerations due to their adjusted design [15–18].

The Unity MR-linac system (Elekta AB, Stockholm, Sweden), based on a Philips 1.5 T Ingenia MRI, is a hybrid system that can be used for quantitative MRI [19]. To allow accurate radiation treatment, adjustments have been made to the MRI part of the system [15], which necessitate special considerations for DWI with the goal of ADC measurements when compared to diagnostic MRI systems. We have identified three main categories for these adjustments: the choice of b-values, the spatial dependence of the ADC for the Unity system, and the influence of the rotating gantry when acquiring data during patient irradiation.

The choice of b-values is influenced by the performance of the gradient system and the available receive coil. Diffusion weighting on the Unity system is performed using the Stejskal-Tanner pulsed gradient spin echo technique, where two balanced diffusion-sensitizing gradients are placed around a 180° refocusing pulse [20]. Either echo planar imaging (EPI), or turbo spin-echo (TSE) can be used for readout. The amount of diffusion weighting depends on the strength, slew rate, and timing of the diffusion gradients and is usually represented by a scalar called the b-value (s/mm^2). The higher the b-value, the stronger the diffusion weighting [20].

The time between the onset of the two diffusion gradients (Δ), sometimes called the diffusion time, is an important parameter for DWI because a longer Δ increases the chance that water molecules reach boundaries in a restricted (biological) environment. Therefore, in structured tissue, a different Δ can result in different ADC values even when the same b-value are used. Normally, Δ is kept as short as possible to minimize T_2 decay and thereby maximizing the SNR. Under clinical operation, the Unity system uses a maximum gradient strength of 15 mT/m and a slew rate of 65 T/m/s, which is lower compared to values typically used in diagnostic systems. Therefore, to achieve the same b-value on a Unity system, the diffusion gradients are prolonged which results in lower SNR and a longer Δ. Figure 1 shows the b-value that corresponds to a particular Δ for the Unity system and a Philips 1.5 T Ingenia scanner, both employing their maximum gradient amplitude and slew rate. To achieve the same Δ, b-values need to be chosen on the Unity that are about half those of diagnostic 1.5 T systems.

Another aspect influencing the choice of b-values is the 2 × 4 channel (four anterior, four posterior) receive coil array [21]. In combination with the gradient performance, this results in a lower SNR when compared to diagnostic systems. As a result of the Rician noise distribution of magnitude images [22], a positive bias is introduced to the measured signal intensities which results in an underestimation of the ADC. This effect becomes larger when the SNR is low warranting careful consideration of the choice of b-values.

The gradient coils of the Unity system are physically split, creating a 22 cm gap around the iso-center to allow passage of the treatment beam [23]. This is different from diagnostic systems and might pose problems for images in the iso-center, especially for DWI where

large diffusion sensitizing gradients are used. For instance, present day gradient systems are actively shielded to reduce the generation of eddy currents in other conductive structures of the MRI. This works well over the area of the gradient coils, but at the edges there is leakage [24]. In diagnostic systems, these edges are away from the iso-center, but for the Unity system they are close to the iso-center due to its split gradient design. This might increase eddy currents which cause unwanted variation in the magnetic field [25]. For DWI, in addition to geometric distortions, this also affects the measured ADC value spatially. Besides eddy currents, there are other sources that can cause spatial variations of ADC values, such as concomitant fields and gradient non-linearity [26–28].

During patient irradiation, a gantry containing the linac rotates around the MRI of the Unity system. Previous studies have shown that the influence of this gantry on the B_0 field is small for both a static gantry at multiple angles [23] and a continuously rotating gantry [29]. It was shown that the inhomogeneities were < 500 nT (or < 0.3 ppm) but varied spatially with the gantry position. It should also be determined if DWI with an EPI readout can be performed during patient irradiation with gantry rotation.

This study is structured around the three categories (choice of b-values, spatial dependence of the ADC, and diffusion measurements during treatment) and the aim is to incorporate system specific considerations regarding these categories in a recommendation for accurate ADC measurement on the Unity system.

Materials and Methods

Choice of b-values

Assuming a mono-exponential decay of the diffusion signal with increasing b-value, the ADC can be calculated using $ADC = \ln\left(S_{b_{low}}/S_{b_{high}}\right)/\left(b_{high} - b_{low}\right)$, where b_{low} and b_{high} are two b-values, with $S_{b_{low}}$ and $S_{b_{high}}$ as corresponding signal intensities. The highest SNR would be obtained when $b_{low} = 0$ s/mm^2 is used. However, besides diffusion, perfusion also attributes to the signal attenuation of DWI, especially at lower b-values [30]. When $b_{low} = 0$ s/mm^2 is used for ADC calculation, the attenuation from perfusion is fully included in the ADC, resulting in an overestimation of the diffusion. Our recommendation focuses on the measurement of water mobility in the extravascular space, which implies that perfusion effects should be excluded from the ADC. To reduce this perfusion bias, a non-zero b_{low} should be used [12,31].

There is no straightforward way to determine the exact b_{low} that should be used, as this depends on the tissue properties that are measured. As an example here, we take prostate tissue and calculate the contribution of perfusion to the total signal for a set of b-values, using the intravoxel incoherent motion model and taking differences in tissue and blood relaxation parameters into account [32]. Tissue T_1 and T_2 were set to 1317 and 88 ms using the 1.5T values reported in [33], and blood T_1 and T_2 were set to 1441 and 290 ms [32]. The ADC, pseudo-diffusion coefficient, and perfusion fraction were 1.34×10^{-3} mm^2/s, 21.1×10^{-3} mm^2/s, and 0.23 respectively [34]. The echo time (TE) and repetition time (TR) were taken from the Unity MR-linac, with the acquisition settings as shown in Supplemental

Table S1. To maximize the gradient performance, a setting called ‘gradient overplus’, which employs the simultaneous application of multiple gradients for diffusion weighting, was used. From these simulations, we observed that at a b-value of 50 s/mm^2, perfusion constitutes 14% of the total signal, which went down to 5% at 100 s/mm^2 and 2% at 150 s/mm^2.

To illustrate how the SNR depends on the b-value on the Unity system, we measured a series of DWIs in a prostate cancer patient, where we increased the b-value from 50 to 1200 s/mm^2 in steps of 50 s/mm^2, while keeping the TE and TR to minimal values, reflecting clinical practice. The b-values were each measured once (no averages). Other imaging parameters can be found in Supplemental Table S1. A noise scan with identical imaging and reconstruction parameters as the scan with b = 500 s/mm^2, was acquired by turning the RF pulses off, which is an available research option. The SNR was calculated within the prostate for all b-values using SNR = S_b/S_n, where S_b is the mean signal in the prostate of the b-value images, and S_n is the mean in the prostate of the noise image.

Spatial dependence of the ADC

To assess the spatial dependence of the ADC, we acquired DWI data using a cylindrical phantom with a 40 cm diameter, containing a copper sulphate solution (Philips Healthcare, Best, The Netherlands) on six Unity systems, and one diagnostic 3T Philips Ingenia for comparison. DWIs were acquired with b-values of 0, 150, and 500 s/mm^2, using a turbo-spin echo (TSE) acquisition without averaging. The voxel size was 4 × 4 × 5 mm and scans were made both with and without using gradient overplus (Supplemental Table S2). Each scan was performed four times on each system for a total of 48 scans (24 without gradient overplus, and 24 with). ADC maps were calculated using the trace images of all b-values, but also from images acquired with employing a single gradient coil (x, y, or z). Here x denotes the left-right direction, y the anterior-posterior direction, and z the cranial-caudal direction for a patient laying on his back. All b-values were used because these measurements are done on a phantom where perfusion is not present. To determine the extent to which gradient nonlinearities influence the spatial variation of diffusion weighting, we applied an offline correction using a spherical harmonics expansion that describes the gradients of the Unity system [27]. The scans were repeated with a smaller phantom (15 cm diameter) containing a copper sulphate solution on a single Unity system using the same EPI readout.

Diffusion measurements during treatment

To determine if acquiring a DWI during treatment influences the ADC values, we imaged 11 prostate cancer patients. On two consecutive treatment days, a T_2-weighed (T_2w) anatomical image, a B_0 map, and two diffusion-weighted images were acquired, one before and one during irradiation (indicated as ‘gantry off’ and ‘gantry on’ below). Acquisition details can be found in Supplemental Table S3. For these specific measurements, the DWI acquisition time was kept below 3:30 minutes by reducing the number of averages, so each acquisition would fit within the irradiation time window. For the calculation of the ADC map, the b = 150 s/mm^2 and b = 500 s/mm^2 images were used.

The prostate and tumors were delineated on the T_2w image of the first fraction, and the tumor boundaries were checked by a radiation oncologist consulting clinical information including pre-treatment multi-parametric MRI. Some patients had multiple lesions, which were considered individually, giving a total of 11 prostates and 15 lesions. The b = 0 s/mm^2 images were registered rigidly to the T_2w images acquired during the same treatment fraction, and this registration was propagated to the ADC maps. Then, the T_2w image of the second fraction was registered deformably to the T_2w image of the first fraction. This registration was then propagated to the ADC maps of the second fraction. After registration, the delineations were propagated to all the separate images, and mean values were used for further analysis.

The mean ADC values of the ROIs were compared using Bland-Altman analysis for four situations: (a) fraction 1 – fraction 2 with gantry off, (b) fraction 1 – fraction 2 with gantry on, (c) gantry on – gantry off during fraction 1, and (d) gantry on – gantry off during fraction 2. The repeatability coefficient (RC) was calculated from the within-subject standard deviation of these four situations by multiplying it by 2.77 [35]. Confidence intervals for these repeatability coefficients were calculated using the χ^2 distribution according to [36].

To determine the influence of the gantry on the accuracy of the ADC values, we scanned the QIBA recommended diffusion phantom (Diffusion Phantom Model 128, High Precision Devices, Inc, Boulder, Colorado) using acquisition parameters as described in the QIBA diffusion profile for measuring this phantom at 1.5T [13]. The phantom was scanned three times, once with a static gantry, once while irradiating the phantom with an IMRT plan, and once while forcing the gantry to move continuously. The median accuracy for these situations was calculated as the percent error compared to the known diffusion values of the phantom.

Patient example

As a patient example of DWI and ADC image quality on the Unity system, we acquired a DWI of a rectal cancer patient following the acquisition settings that are presented as a result of the current study. The acquisition voxel size was 4 × 4 × 5 mm^3, and b-values of 150 and 500 s/mm^2 were used, with 4 and 16 averages respectively (Supplemental Table S4).

The patient studies were approved by the medical ethics committee of the Netherlands Cancer Institute and written informed consent was obtained.

Results

Figure 2 shows in vivo results of the SNR measurement, including a plot of the SNR as a function of increasing b-value (and TE) in the prostate (Figure 2h). The SNR is 10.0 at b=50 s/mm^2 and decreases with an increasing b-value and TE. To illustrate, the SNR at b=500 s/mm^2 is 3.8 and at b=1000 s/mm^2 is 1.7. ADC values in the prostate, calculated from these scans using their corresponding b=0 s/mm^2 images (with the same TE) were 1.82 and 1.59 × 10^{-3} mm^2/s.

A distinct spatial pattern appears in the ADC maps of the homogeneous diffusion phantom. Figure 3 a–c shows when individual gradient coils are used for diffusion weighting. The most severe increase in ADC was found when using only the y-direction coil (Figure 3b). No spatial pattern was present when only using the z-direction gradient coil for diffusion weighting (Figure 3c). For both the trace image with and without gradient overplus (Figure 3 d and e), the spatial pattern is present. In the most extreme case, the ADC value went up to 13×10^{-3} mm^2/s, which is an increase of more than 600% compared to the mean ADC of a ROI in the iso-center. The extent of the spatial variation is slightly less when gradient overplus is not used. Similar results were found on all six Unity systems (Supplemental Figure S1). This spatial pattern was not present on the 3T Philips Ingenia system, which showed a much more homogeneous result, especially after the gradient nonlinearity correction (Supplemental Figure S2b and d). The smaller phantom imaged with an EPI readout showed results consistent with the same region in the TSE scans (Supplemental Figure S3).

Bland-Altman plots of the ADC measurements before and during irradiation are shown in Figure 4, where mean values from the prostate and lesion delineations are shown. Figure 4a indicates the day-to-day variability under normal conditions, with the gantry turned off. The repeatability coefficients for the four situations (Figure 4 a–d), including 95% confidence intervals were 0.09 (0.06–0.15), 0.07 (0.05–0.11), 0.08 (0.06–0.13), and 0.07 (0.05–0.11) × 10^{-3} mm^2/s for the prostate, showing similar results for cases before and during treatment. For the tumors, the values were 0.37 (0.26–0.63), 0.31 (0.22–0.52), 0.34 (0.24–0.57), and 0.22 (0.16–0.38) × 10^{-3} mm^2/s.

For the accuracy measurements with the diffusion phantom, the median accuracy with a static gantry was 1.1%, while irradiating the phantom with an IMRT plan was 0.5%, and with a continuously rotating gantry was 1.3%. A Bland-Altman plot with the individual data points can be found in Supplemental Figure S4.

A representative example of images of a rectal cancer patient is shown in Figure 5, including an ADC map in Figure 5c.

Discussion

The adjusted design of the Unity system results in differences in DWI compared to diagnostic MR scanners. For this, we identified three main categories: the choice of b-values, the spatial dependence of the ADC, and diffusion measurements during treatment. Based on our experiments, simulations, and existing literature, we give recommendations for the Unity system.

It is important to realize that the calculated ADC depends on the choice of b-values and therefore should be homogenized among centers to enable comparison. To exclude perfusion from the ADC, a b_{low} value of 100 – 150 s/mm^2 should be used, in line with what is recommended in [12]. Ideally this should be tailored to the tissue of interest. We show an example calculation to estimate the perfusion bias which could be used to guide the decision for the b_{low} when designing a trial.

The choice to limit the b_{high} value is mainly based on the difference in Δ as showed in Figure 1. To establish the ADC as a response biomarker, the reproducibility among different systems is important. A sequence with a different Δ leads to different ADC values in structured tissues even when the same b-values are used. Rather than measuring at the same b-value, one should make an effort to measure at a similar Δ. To facilitate the comparison among different systems, the Δ should be reported. Furthermore, trials to compare ADC values from MR-linacs to diagnostic systems should be performed.

Other factors that limit the b_{max} are the reduced SNR, the gradient performance, and the available acquisition time. To reduce the bias in the ADC value caused by Rician noise, it is important to verify, for instance in a volunteer, that the b_{high} measurement has sufficient SNR. Note here that the SNR in the target area usually also depends on body size. If the SNR needs to be improved, one or a combination of the following parameters should be changed: increasing the acquisition voxel size, lowering the SENSE encoding factor or lowering the partial Fourier imaging factor. These latter two should be considered on a tissue basis as they increase the TE, potentially also decreasing the SNR due to T_2-decay. While increasing the number of averages for the b-values yields a more homogeneous image by reducing random signal intensity fluctuations, the ADC bias will not be reduced [37]. The total number of averages that can be acquired depend on the total acquisition time that is available. Once the total number of averages is chosen, the b_{high} images should be acquired three to four times as often as the b_{low} images [38,39].

Taking the Δ and these other factors into consideration, we propose that a maximum b_{high} of 500 s/mm^2 should be used for ADC measurements on the Unity system. It is important to note that on the Unity system, the Δ of a specific DWI sequence depends on the highest b-value acquired in that sequence. Therefore, adding additional b-values above the recommended 500 s/mm^2 to the sequence will increase the Δ and result in a different ADC value even when the ADC is calculated from the b = 500 s/mm^2 image.

ADC maps on the Unity system contain severe spatial variations, even when homogeneous solutions are used for measurements. Although these variations are more present in the trace ADC map acquired with gradient overplus (compared to the trace ADC map without, Figure 4e and 4d, respectively), we recommend scanning with this setting for its benefit of reduced TE and therefore increased SNR. The spatial dependence of the diffusion weighting is well documented in diagnostic systems where it is largely explained by gradient nonlinearity (see Supplemental Figure S2b and S2d) [28]. However, applying the offline gradient nonlinearity correction only resulted in a negligible change of the spatial variation (compare Supplemental Figure S2a to S2c). We therefore hypothesize that on the Unity system, the spatial variation is caused by increased eddy currents resulting from the split gradient coil design. Accurate ADC determination is possible within a radius of 7 cm from the iso-center, depicted as the circle in Figure 3g. Further research is needed to investigate if corrections of the distortions away from the iso-center are feasible.

Eddy current distortions depend on the gradient coils that are used. As visible in Supplemental Figure S1, the y-direction gradient has the poorest characteristics for DWI. Also, when only using the z-direction gradient coil (Figure 4c, Figure S1 row 3), no spatial

variation was present. Using only this coil could be an option for acquiring DWIs in patients that have tumor sites far outside the iso-center (in the axial plane) and are therefore impacted by the spatial dependence present in the trace images. However, unless the measured diffusion is isotropic, the resulting ADC would differ from the trace ADC.

We were unable to scan the large body phantom with an EPI readout, because in order to position the phantom, the posterior coil must be removed. Therefore, parallel imaging was unavailable resulting in severe distortions due to a low bandwidth. We showed with a smaller phantom that our recommendation to scan within 7 cm from the iso-center holds for EPI readouts.

Scanning DWI during patient during gantry rotation did not affect the ADC values. The accuracy of the ADC values in the diffusion phantom was comparable between measuring with a static and with a rotating gantry. A similar RC was found when comparing scanning before and during treatment to day-to-day repeatability, and the bias in the Bland-Altman plots for cases c and d (comparing static to moving gantry) were 0.02 and 0.00×10^{-3} mm^2/s, respectively. Hence, DWI could be acquired at any available time during treatment to facilitate an optimal MRI protocol during each fraction.

In summary, our Unity system specific recommendations include limiting the b_{high} to 500 s/mm^2, scanning a target within 7 cm of the iso-center, and that measuring the ADC during treatment delivery is possible. Table 1 provides an overview of these recommendations, including example acquisition parameters to be used with the goal of measuring the ADC accurately.

The QIBA recommendations for DWI includes the need for test-retest studies in order to calculate the repeatability coefficient [35]. This should be used to establish clinical confidence in the ADC QIB and to help interpret the results from treatment response monitoring and outcome prediction studies. We also emphasize that test-retest studies should be the next step for DWI studies on Unity.

In conclusion, we provide recommendations for DWI on the Unity system, incorporating hardware specific considerations. These recommendations provide a basis for test-retest studies and, when used, will facilitate multi-center biomarker studies and future meta-analyses.

Supplementary Material

Refer to Web version on PubMed Central for supplementary material.

Acknowledgments

MN declares travel support from Elekta AB. DT declares institutional collaborations with Elekta, Philips, Siemens and PTW Freiburg outside of this work. The Tübingen MR-linac program is funded by the German Research Council (DFG), grants no. ZI 736/2-1 and TH 1528/6-1. The UMCU has a long-standing research relation with Elekta and Philips. The MCW receives departmental research and travel support from Elekta. EP declares funding support from Elekta Instruments AB. UH receives research funding from Elekta AB and Philips Healthcare and ITEA project ‘Starlit’.

References

[1]. Gurney-Champion OJ, Mahmood F, van Schie M, Julian R, George B, Philippens MEP, et al. Quantitative imaging for radiotherapy purposes. Radiother Oncol 2020;146:66–75. doi:10.1016/j.radonc.2020.01.026. [PubMed: 32114268]

[2]. Keenan KE, Biller JR, Delfino JG, Boss MA, Does MD, Evelhoch JL, et al. Recommendations towards standards for quantitative MRI (qMRI) and outstanding needs. J Magn Reson Imaging 2019;49:e26–39. doi:10.1002/jmri.26598. [PubMed: 30680836]

[3]. Keenan KE, Ainslie M, Barker AJ, Boss MA, Cecil KM, Charles C, et al. Quantitative magnetic resonance imaging phantoms: A review and the need for a system phantom. Magn Reson Med 2017;00. doi:10.1002/mrm.26982.

[4]. O'Connor JPB, Aboagye EO, Adams JE, Aerts HJWL, Barrington SF, Beer AJ, et al. Imaging biomarker roadmap for cancer studies. Nat Rev Clin Oncol 2017;14:169–86. doi:10.1038/nrclinonc.2016.162. [PubMed: 27725679]

[5]. Obuchowski NA, Buckler A, Kinahan P, Chen-Mayer H, Petrick N, Barboriak DP, et al. Statistical Issues in Testing Conformance with the Quantitative Imaging Biomarker Alliance (QIBA) Profile Claims. Acad Radiol 2016;23:496–506. doi:10.1016/j.acra.2015.12.020. [PubMed: 26898527]

[6]. Mahmood F, Johannesen HH, Geertsen P, Hansen RH. Repeated diffusion MRI reveals earliest time point for stratification of radiotherapy response in brain metastases. Phys Med Biol 2017;62:2990–3002. doi:10.1088/1361-6560/aa5249. [PubMed: 28306548]

[7]. Yang Y, Cao M, Sheng K, Gao Y, Chen A, Kamrava M, et al. Longitudinal diffusion MRI for treatment response assessment: Preliminary experience using an MRI-guided tri-cobalt 60 radiotherapy system. Med Phys 2016;43:1369–73. doi:10.1118/1.4942381. [PubMed: 26936721]

[8]. Lambrecht M, Vandecaveye V, De Keyzer F, Roels S, Penninckx F, Van Cutsem E, et al. Value of diffusion-weighted magnetic resonance imaging for prediction and early assessment of response to neoadjuvant radiochemotherapy in rectal cancer: Preliminary results. Int J Radiat Oncol Biol Phys 2012;82:863–70. doi:10.1016/j.ijrobp.2010.12.063. [PubMed: 21398048]

[9]. Lambrecht M, Van Herck H, De Keyzer F, Vandecaveye V, Slagmolen P, Suetens P, et al. Redefining the target early during treatment. Can we visualize regional differences within the target volume using sequential diffusion weighted MRI? Radiother Oncol 2014;110:329–34. doi:10.1016/j.radonc.2013.09.023. [PubMed: 24231234]

[10]. Park SY, Kim CK, Park BK, Park W, Park HC, Han DH, et al. Early changes in apparent diffusion coefficient from diffusion-weighted MR imaging during radiotherapy for prostate cancer. Int J Radiat Oncol Biol Phys 2012;83:749–55. doi:10.1016/j.ijrobp.2011.06.2009. [PubMed: 22154286]

[11]. Liu Y, Bai R, Sun H, Liu H, Zhao X, Li Y. Diffusion-weighted imaging in predicting and monitoring the response of uterine cervical cancer to combined chemoradiation. Clin Radiol 2009;64:1067–74. doi:10.1016/j.crad.2009.07.010. [PubMed: 19822239]

[12]. Padhani AR, Liu G, Mu-Koh D, Chenevert TL, Thoeny HC, Takahara T, et al. Diffusion-Weighted Magnetic Resonance Imaging as a Cancer Biomarker: Consensus and Recommendations. Neoplasia 2009;11:102–25. doi:10.1593/neo.81328. [PubMed: 19186405]

[13]. Perfusion, Diffusion and Flow-MRI Biomarker Committee. QIBA Profile: Diffusion-Weighted Magnetic Resonance Imaging (DWI). Public comment draft. QIBA 2019.

[14]. Baltzer AP, Mann RM, Iima M, Sigmund EE, Clauser P, Gilbert F. Diffusion-Weighted Imaging of the breast – A consensus and mission statement from the EUSOBI International Breast Diffusion- Weighted Imaging working group 2019:1–25.

[15]. Raaymakers BW, Lagendijk JJW, Overweg J, Kok JGM, Raaijmakers AJE, Kerkhof EM, et al. Integrating a 1.5 T MRI scanner with a 6 MV accelerator: proof of concept. Phys Med Biol 2009;54:N229–37. doi:10.1088/0031-9155/54/12/N01. [PubMed: 19451689]

[16]. Mutic S, Dempsey JF. The ViewRay System: Magnetic Resonance-Guided and Controlled Radiotherapy. Semin Radiat Oncol 2014;24:196–9. doi:10.1016/j.semradonc.2014.02.008. [PubMed: 24931092]

[17]. Fallone BG. The Rotating Biplanar Linac-Magnetic Resonance Imaging System. Semin Radiat Oncol 2014;24:200–2. doi:10.1016/j.semradonc.2014.02.011. [PubMed: 24931093]

[18]. Keall PJ, Barton M, Crozier S. The Australian Magnetic Resonance Imaging-Linac Program. Semin Radiat Oncol 2014;24:203–6. doi:10.1016/j.semradonc.2014.02.015. [PubMed: 24931094]

[19]. Kooreman ES, van Houdt PJ, Nowee ME, van Pelt VWJ, Tijssen RHN, Paulson ES, et al. Feasibility and accuracy of quantitative imaging on a 1.5 T MR-linear accelerator. Radiother Oncol 2019;133:156–62. doi:10.1016/j.radonc.2019.01.011. [PubMed: 30935572]

[20]. Stejskal EO, Tanner JE. Spin diffusion measurements: Spin echoes in the presence of a time-dependent field gradient. J Chem Phys 1965;42:288–92. doi:10.1063/1.1695690.

[21]. Hoogcarspel SJ, Zijlema SE, Tijssen RHN, Kerkmeijer LGW, Jürgenliemk-Schulz IM, Lagendijk JJW, et al. Characterization of the first RF coil dedicated to 1.5 T MR guided radiotherapy. Phys Med Biol 2018;63. doi:10.1088/1361-6560/aaa303.

[22]. Gudbjartsson H, Patz S. The Rician distribution of noisy MRI data (vol 34, pg 910, 1995). Magn Reson Med 1996;36:332.

[23]. Tijssen RHN, Philippens MEP, Paulson ES, Glitzner M, Chugh B, Wetscherek A, et al. MRI commissioning of 1 . 5T MR-linac systems – a multi-institutional study. Radiother Oncol 2019;132:114–20. doi:10.1016/j.radonc.2018.12.011. [PubMed: 30825959]

[24]. Baig TN, Eagan TP, Petropoulos LS, Kidane TK, Edelstein WA, Brown RW. Gradient coil with active endcap shielding. Concepts Magn Reson Part B Magn Reson Eng 2007;31B:12–23. doi:10.1002/cmr.b.20079.

[25]. Chan RW, Von Deuster C, Giese D, Stoeck CT, Harmer J, Aitken AP, et al. Characterization and correction of eddy-current artifacts in unipolar and bipolar diffusion sequences using magnetic field monitoring. J Magn Reson 2014;244:74–84. doi:10.1016/j.jmr.2014.04.018. [PubMed: 24880880]

[26]. Meier C, Zwanger M, Feiweier T, Porter D. Concomitant field terms for asymmetric gradient coils: Consequences for diffusion, flow, and echo-planar imaging. Magn Reson Med 2008;60:128–34. doi:10.1002/mrm.21615. [PubMed: 18581353]

[27]. Bammer R, Markl M, Barnett A, Acar B, Alley MT, Pelc NJ, et al. Analysis and generalized correction of the effect of spatial gradient field distortions in diffusion-weighted imaging. Magn Reson Med 2003;50:560–9. doi:10.1002/mrm.10545. [PubMed: 12939764]

[28]. Malyarenko D, Galbán CJ, Londy FJ, Meyer CR, Johnson TD, Rehemtulla A, et al. Multi-system repeatability and reproducibility of apparent diffusion coefficient measurement using an ice-water phantom. J Magn Reson Imaging 2013;37:1238–46. doi:10.1002/jmri.23825. [PubMed: 23023785]

[29]. Jackson SJ, Glitzner M, Tijssen RHN, Raaymakers BW. MRI B_0 homogeneity and geometric distortion with continuous linac gantry rotation on an Elekta Unity MR-linac. Phys Med Biol 2019:0–7. doi:10.1088/1361-6560/ab231a.

[30]. Le Bihan D, Breton E, Lallemand D, Grenier P, Cabanis E, Laval-Jeantet M. MR imaging of intravoxel incoherent motions: application to diffusion and perfusion in neurologic disorders. Radiology 1986;161:401–7. doi:10.1148/radiology.161.2.3763909. [PubMed: 3763909]

[31]. Le Bihan D What can we see with IVIM MRI? Neuroimage 2018:1–12. doi:10.1016/j.neuroimage.2017.12.062.

[32]. Lemke A, Laun FB, Simon D, Stieltjes B, Schad LR. An in vivo verification of the intravoxel incoherent motion effect in diffusion-weighted imaging of the abdomen. Magn Reson Med 2010;64:1580–5. doi:10.1002/mrm.22565. [PubMed: 20665824]

[33]. de Bazelaire CMJ, Duhamel GD, Rofsky NM, Alsop DC. MR Imaging Relaxation Times of Abdominal and Pelvic Tissues Measured in Vivo at 3.0 T: Preliminary Results. Radiology 2004;230:652–9. doi:10.1148/radiol.2303021331. [PubMed: 14990831]

[34]. Riches SF, Hawtin K, Charles-Edwards EM, de Souza NM. Diffusion-weighted imaging of the prostate and rectal wall: Comparison of biexponential and monoexponential modelled diffusion and associated perfusion coefficients. NMR Biomed 2009;22:318–25. doi:10.1002/nbm.1328. [PubMed: 19009566]

[35]. Shukla-Dave A, Obuchowski NA, Chenevert TL, Jambawalikar S, Schwartz LH, Malyarenko D, et al. Quantitative imaging biomarkers alliance (QIBA) recommendations for improved precision

of DWI and DCE-MRI derived biomarkers in multicenter oncology trials. J Magn Reson Imaging 2018. doi:10.1002/jmri.26518.

[36]. Barnhart HX, Barboriak DP. Applications of the repeatability of quantitative imaging biomarkers: a review of statistical analysis of repeat data sets. Transl Oncol 2009;2:231–5. doi:10.1593/tlo.09268. [PubMed: 19956383]

[37]. Dietrich O, Heiland S, Sartor K. Noise correction for the exact determination of apparent diffusion coefficients at low SNR. Magn Reson Med 2001;45:448–53. doi:10.1002/1522-2594(200103)45:3<448::AID-MRM1059>3.0.CO;2-W. [PubMed: 11241703]

[38]. Bito Y, Hirata S, Yamamoto E. Optimal gradient factors for ADC measurements. B. Abstr. Third Annu. Meet. Int. Soc. Magn. Resnance Med. ISMRM, Berkeley, CA: ISMRM; 1995, p. 913.

[39]. Saritas EU, Lee JH, Nishimura DG. SNR dependence of optimal parameters for apparent diffusion coefficient measurements. IEEE Trans Med Imaging 2011;30:424–37. doi:10.1109/TMI.2010.2084583. [PubMed: 20934948]

- Machine characteristics must be considered when selecting b-values for measuring the ADC
- Spatial variation of the ADC requires positioning of a ROI near the iso-center
- The ADC can be measured on the Unity system during gantry rotation and irradiation
- Includes example acquisition parameters to facilitate multi-center research

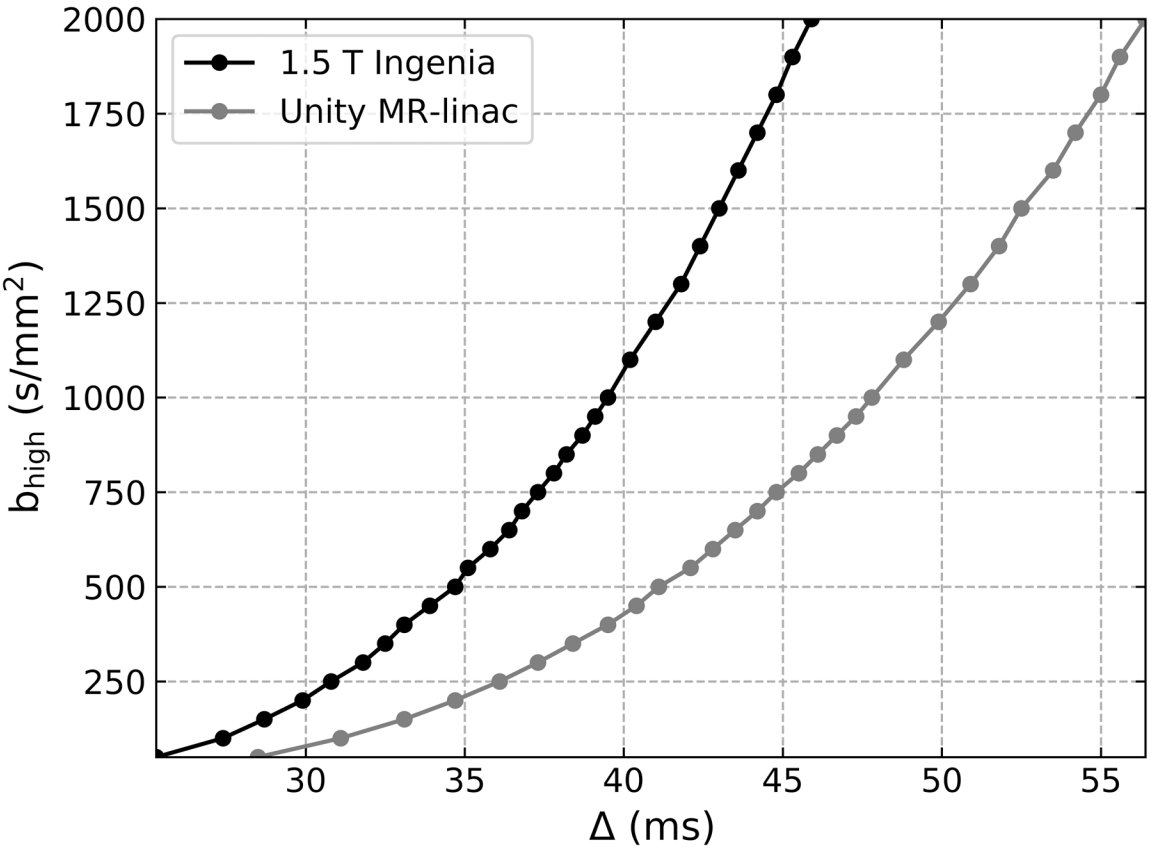

Figure 1:

Comparison of Δ between the Unity system and a 1.5T Philips Ingenia. This is the time between the start of the two diffusion gradients. For example, a b-value of 1200 s/mm^2 at the diagnostic system has a Δ of 41 ms. For the Unity system, the b-value with this same Δ is less than half: 500 s/mm^2.

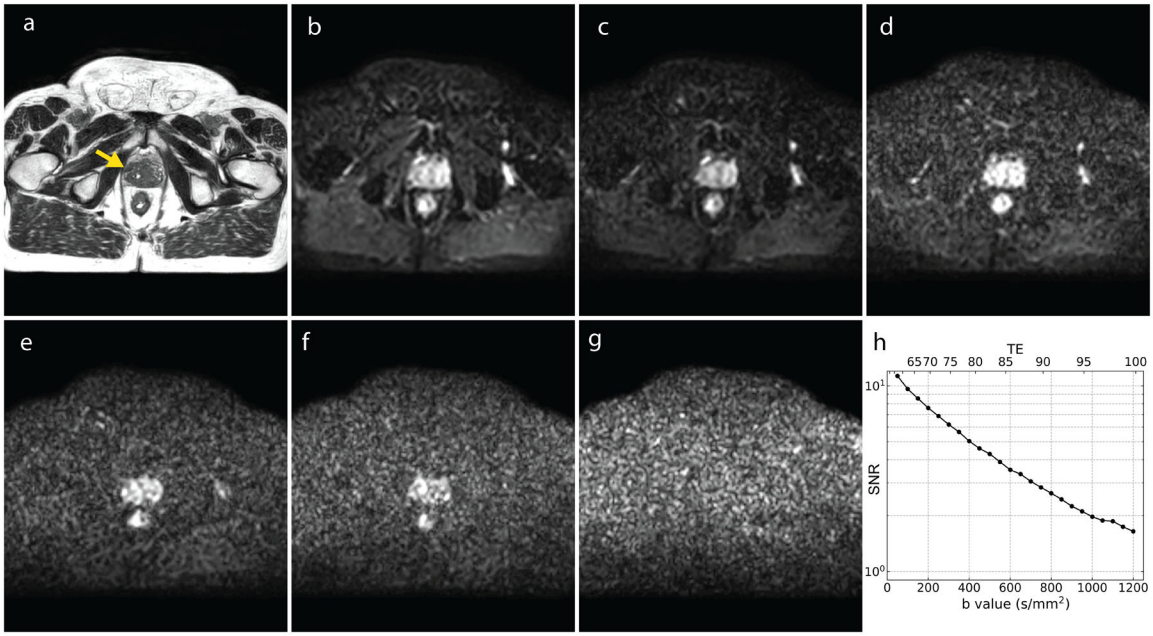

Figure 2:

In vivo data of the prostate cancer patient SNR measurement. (a) T_2w image, the yellow arrow indicates the location of the tumor. (b-f) DWI with an increasing b-value (100, 250, 500, 750, and 1000 s/mm^2), acquired without averaging. The window/level of these images are decreased to facilitate the reduction in signal. Note that disappearance of surrounding structures with an increase in b-value, indicating a reduction in SNR. (g) Noise map of the patient. (h) SNR of the prostate ROI as a function of b-value (and TE).

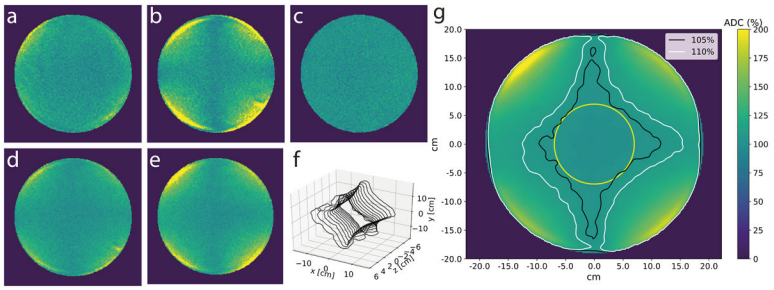

Figure 3:

ADC maps of a large cylindrical phantom, acquired with employing different gradient combinations. The phantom is placed axially and the slice in the iso-center (z=0) is shown. (a-e) ADC maps obtained when using single gradient directions, x, y, and z, respectively. (d) Trace ADC map combining (a-c). (e) Trace ADC map acquired while using gradient overplus. (g) A smoothed average image of the acquisitions of all six MR-linacs, with gradient overplus. The contours represent the regions within which the ADC increase is less than 5%, and less than 10% when compared to the ADC value in the center. This results in a diamond shape with a diagonal length of ~20 cm for the 5% contour. The circle in the middle has a radius of 7 cm. (f) 3D representation of the 5% contour for multiple slices of the body phantom, showing a diamond centered at the isocenter, which increases in size when moving outwards in the z-direction.

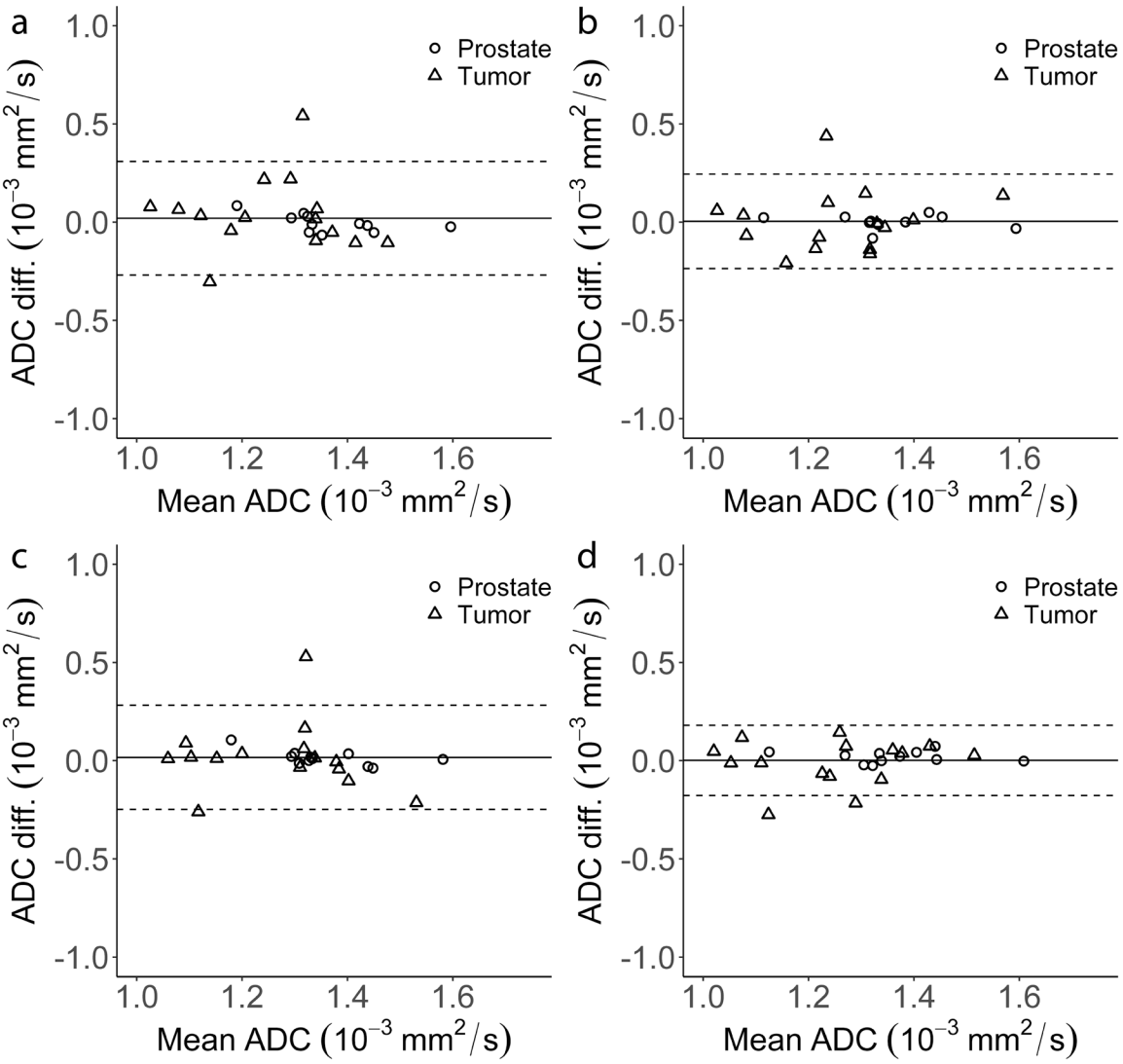

Figure 4:

Bland-Altman plots of the four ADC measurements acquired on consecutive days and before and during treatment. (a) fraction 1 – fraction 2 gantry off, (b) fraction 1 – fraction 2 gantry on, (c) gantry on – gantry off fraction 1, (d) gantry on – gantry off fraction 2. The bias and limits of agreement of a-d are 0.02 (−0.27 – 0.31), 0.00 (−0.24 – 0.25), 0.02 (−0.25 – 0.28), and 0.00 (−0.18 – 0.18) × 10^{-3} mm^2/s.

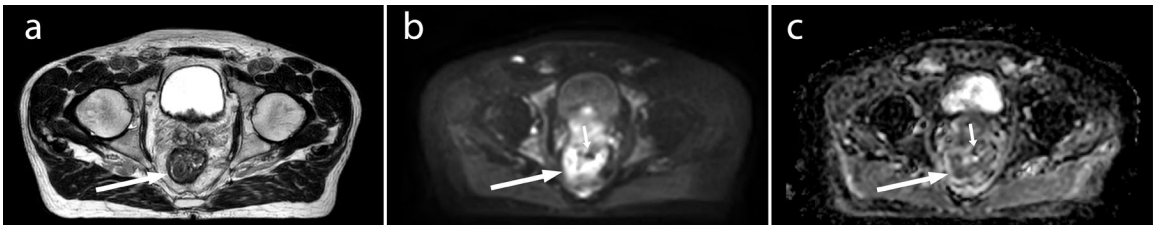

Figure 5:

Representative example of a rectal cancer patient. a) T_2-weighted image, b) DWI b = 500 s/mm^2 image, and c) ADC map. The large white arrows indicate the location of the tumor. On the DWI and ADC images, the tumor shape is slightly deformed due to the presence of air (small arrows).

Table 1:

Acquisition parameters for ADC measurements on the Unity system.

Topic	Recommendations for ADC measurements at the Unity system	Comments
Highest b-value	500 s/mm^2	
Spatial dependence of the ADC	< 7 cm of the iso-center in the x and y direction. Outside this volume the ADC depends heavily on position.	Only using the z-direction gradient coils can be considered when ROI is > 7 cm outside iso-center (axially).
Treatment delivery	ADC measurements can be done during treatment delivery	
	Example parameters that could serve as a starting point	
Acquisition Sequence	SS-EPI	SS-EPI should be used for its speed and SNR benefit.
Lipid Suppression	On	
Slice thickness (mm)	3–5	Ensure sufficient SNR in the b_{high} image.
Gap thickness (mm)	0–1	A gap thickness of 0 should only be used if slices are acquired in an interleaved fashion.
In plane resolution (mm)	1–5	
Phase encoding direction	Choose the direction which causes the least distortions to the tumor site.	
Bandwidth (Hz/pixel)	Max possible in phase encoding direction.	Can be increased by increasing the SENSE factor.
Lowest b-value (other than b=0 s/mm^2)	100 – 150 s/mm^2	Depending on target site. The b=0 s/mm^2 image should not be used for ADC calculation.
Number of signal averages	The highest b-value should be acquired 3–4 times as often as the lowest.	Based on [36–38].
Echo time	Shortest	Gradient overplus should be used to reduce the echo time.
SENSE	0 – 2.5x	Higher SENSE reduces geometric distortions, but also reduces SNR.
Partial Fourier (half-scan)	0.6 – 1	Using half-scan reduces SNR.